Received August 2000
Revised November 2000
Accepted November 2000

# Laminar forced convection heat transfer from a cylinder covered with an orthotropic porous layer in cross-flow

Bassam A/K Abu-Hijleh
*Department of Mechanical Engineering, Jordan University of Science & Technology, Jordan*

***Keywords*** *Laminar flow, Forced convection, Heat transfer, Cylinders*

***Abstract*** *The problem of laminar cross-flow forced convection heat transfer from a horizontal cylinder covered with an orthotropic porous layer was investigated numerically. The effects of porous layer thickness, radial resistance, tangential resistance, and incoming flow Reynolds number on the average Nusselt number were studied in detail. There was up to 40 per cent reduction in the average Nusselt number at high values of Reynolds number. The tangential resistance effect on the Nusselt number was dominant over that of the radial resistance. The effectiveness of the porous layer increased at high values of porous layer thickness as well as at high values of Reynolds number.*

## Nomenclature

E = parameter in computational domain, $\pi\, e^{\pi\xi}$
g = gravity
h = local convection heat transfer coefficient
$K_r$ = non-dimensional pressure loss coefficient in the radial direction
$K_\theta$ = non-dimensional pressure loss coefficient in the tangential direction
k = conduction heat transfer coefficient
M = number of grid points in the tangential direction
N = number of grid points in the radial direction
$\overline{Nu_D}(\theta)$ = local Nusselt number based on cylinder diameter, no porous layer
$\overline{Nu_D}$ = average Nusselt number based on cylinder diameter, no porous layer
$\overline{Nu_{D,P}}$ = average Nusselt number based on cylinder diameter, with porous layer
P = non-dimensional pressure
p = pressure
Pr = Prandtl number
R = non-dimensional radius
r = radius
Re = Reynolds number based on cylinder radius
$Re_D$ = Reynolds number based on cylinder diameter
T = temperature
U = non-dimensional radial velocity
u = radial velocity
V = non-dimensional tangential velocity
v = tangential velocity

*Greek letters*

$\alpha$ = thermal diffusivity
$\beta$ = coefficient of thermal expansion
$\in$ = measure of convergence of numerical results
$\eta$ = independent parameter in computational domain representing tangential direction
$\theta$ = angle measured from bottom
$\nu$ = kinematic viscosity
$\xi$ = independent parameter in computational domain representing radial direction
$\rho$ = density
$\phi$ = non-dimensional temperature
$\psi$ = stream function
$\omega$ = vorticity function

*Subscripts*

D = value based on cylinder diameter
o = value at cylinder surface
p = porous layer
$\infty$ = free stream value

International Journal of Numerical Methods for Heat & Fluid Flow, Vol. 11 No. 2, 2001, pp. 106-120.

## Introduction

Laminar forced convection cross-flow heat transfer from a heated cylinder is an important problem in heat transfer. It is used to simulate a wide range of engineering applications as well as provide a better insight into more complex systems of heat transfer. Accurate knowledge of the overall convection heat transfer around circular cylinders is important in many fields, including heat exchangers, hot water and steam pipes, heaters, refrigerators and electrical conductors. Because of its industrial importance, this class of heat transfer has been the subject of many experimental and analytical studies since the early work of Morgan (1975) and continues until today. Recent economic and environmental concerns have raised interest in methods of reducing or increasing convection heat transfer, depending on the application, from a horizontal cylinder. Classical methods such as the use of insulation materials are becoming a cost as well as an environmental concern. Researchers continue to look for new methods of heat transfer control. Several researchers studied the potential of using porous material to increase (Al-Nimr and Alkam, 1998; Zhang and Zhao, 2000) or decrease (Huang and Vafai, 1994; Abu-Hijleh, n.d.) the heat transfer characteristics in several other configurations. A comprehensive roundup of work in this area can be found in a recent paper by Alazmi and Vafai (2000).

This paper presents the numerical results of using an orthotropic porous layer on the cylinder's outer surface in order to reduce the forced convection heat transfer from a cylinder in cross-flow. The use of an orthotropic porous layer allows the designer to optimize the thermal characteristics of an insulation material in a fashion similar to that used to tailor the mechanical properties of composite materials. The fluid under consideration is air. The numerical solution of the elliptic momentum and energy equations was performed using the stream function-vorticity method on a stretched grid. This detailed study included varying the Reynolds number ($Re_D$) from 1 to 200, non-dimensional porous layer radius ($R_p$) from 1.1 to 2.0, and non-dimensional radial and tangential porous layer resistances ($K_r$ and $K_\theta$, respectively) from 0.25 to 2.0.

## Mathematical analysis

The steady-state equations for 2D laminar forced convection over a horizontal cylinder are given by:

$$\frac{1}{r}\frac{\partial(ru)}{\partial r}+\frac{1}{r}\frac{\partial v}{\partial \theta}=0 \tag{1}$$

$$u\frac{\partial u}{\partial r}+\frac{v}{r}\frac{\partial u}{\partial \theta}-\frac{v^2}{r}=\frac{1}{\rho}\frac{\partial P}{\partial r}-K_r^*\frac{u^2}{2}+\nu\left[\frac{\partial^2 u}{\partial r^2}+\frac{1}{r}\frac{\partial u}{\partial r}-\frac{u}{r^2}+\frac{1}{r^2}\frac{\partial^2 u}{\partial \theta^2}-\frac{2}{r^2}\frac{\partial v}{\partial \theta}\right] \tag{2}$$

$$u\frac{\partial v}{\partial r}+\frac{v}{r}\frac{\partial v}{\partial \theta}+\frac{uv}{r}=\frac{1}{\rho}\frac{\partial P}{\partial r}-K^{*}_{\theta}\frac{v^{2}}{2}+\nu\left[\frac{\partial^{2}v}{\partial r^{2}}+\frac{1}{r}\frac{\partial v}{\partial r}-\frac{v}{r^{2}}+\frac{1}{r^{2}}\frac{\partial^{2}v}{\partial \theta^{2}}+\frac{2}{r^{2}}\frac{\partial u}{\partial \theta}\right] \quad (3)$$

$$u\ \frac{\partial T}{\partial r}+\frac{v}{r}\frac{\partial T}{\partial \theta}=\alpha\left(\frac{1}{r}\frac{\partial rT}{\partial r}+\frac{1}{r^{2}}\frac{\partial^{2}T}{\partial \theta^{2}}\right). \quad (4)$$

The second term in equations (2) and (3) represent the extra pressure loss experienced by the flow as it passes through the porous layer. The values of ($K^{*}_{r}$) and ($K^{*}_{\theta}$) have units of ($m^{-1}$) and can be obtained for different materials and configurations in handbooks, most notably the *Handbook of Hydraulic Resistance* by Idelchik (1994). The value of the pressure loss coefficients is set to zero outside the porous layer ($r > r_{p}$). This type of formulation allows for modeling of orthotropic porous layers ($K^{*}_{r} \neq K^{*}_{\theta}$) as well as the more traditional isotropic porous layers ($K^{*}_{r} = K^{*}_{\theta}$). This formulation also allows for the use of a unified set of equations for both the porous layer and the clear fluid. This greatly simplifies the numerical solution of the problem. Switching between the porous layer and the clear fluid is done by setting the pressure loss coefficients to zero outside the porous layer. This negates the need for special treatment at the interface between the porous layer and the clear region. This condition implies that there is a continuity in the velocity, temperature, and shear stress at the interface between the porous layer and the clear fluid (Ochoa-Tapia and Whitaker, 1995a). Some researchers (Ochoa-Tapia and Whitaker, 1995a; 1995b; Kuznetsov, 2000) suggested that there is a jump in the shear stress at the interface. Modelling this jump requires an adjustable coefficient. This coefficient is not universal and needs to be determined from experimental data for the flow being studied. Most researchers until today continue to use the continuity boundary condition at the interface between the porous layer and the clear fluid. In a recent study by Zhang and Zhao (2000), the authors numerically simulated the heat transfer and fluid flow over a backward facing step with a porous insert. The numerical model used in their study employed the continuity boundary condition at the interface between the porous layer and the clear fluid. The numerical results of the local Nusselt number on the floor of the backward facing step compared quite favorably with the results reported by Martin *et al.* (1998) for the same configuration. The authors also performed a comparison with the work of other researchers in which they verified that the model can accurately predict the hydrodynamic flow field. This indicates that the continuity boundary condition at the interface between the porous layer and the clear fluid is suitable for accurate simulation of the hydrodynamic and thermal flow fields in the types of problems such as the problem presented in this paper.

The thermal diffusivity used in equation (4) is that of the fluid, i.e. air. In most cases the thermal diffusivity of the porous material will be different from that of the fluid giving rise to an effective thermal diffusivity within the porous layer (Al-Nimr and Allcam, 1998). In this study it is assumed that the effective

diffusivity does not deviate much from that of air due to the presence of the porous material. This assumption is valid for porous materials with thermal diffusivity close to that of air and/or porous material with low density. Varying the value of the thermal diffusivity means there is an additional parameter that needs to be studied. This would lead to a significant increase in the number of possible permutations and resulting data. Thus the thermal diffusivity was fixed at that of air in this study. The boundary conditions for equations (1-4) are:

(1) On the cylinder surface, i.e. $r = r_o$; $u = v = 0$ and $T = T_o$.

(2) Far-stream from the cylinder, i.e. $r \rightarrow \infty$; $u \rightarrow U_\infty \cos(\theta)$ and $v \rightarrow -U_\infty \sin(\theta)$. As for the temperature, the far-stream boundary condition is divided into an outflow ($\infty \leq 90$ degrees) and an inflow ($\theta > 90$ degrees) regions (Figure 1). The far-stream temperature boundary conditions are $T = T_\infty$ and $\partial T/\partial r = 0$ for the inflow and outflow regions, respectively.

(3) Plane of symmetry; è = 0 and è = 180 degrees; $v = 0$ and $u/è = T/è = 0$.

The local and average Nusselt number, based on diameter, are calculated as:

$$Nu_D(\theta) = \frac{Dh(\theta)}{k}; \overline{Nu_D} = \frac{1}{\pi}\frac{D}{k}\int_0^\pi h(\theta)d\theta = -\frac{D}{\pi}\int_0^\pi \frac{\partial T(r_o,\theta)/\partial r}{(T_o - T_\infty)}\partial\theta. \quad (5)$$

The following non-dimensional groups are introduced:

$$R \equiv \frac{r}{r_o},\ U \equiv \frac{u}{U_\infty},\ V \equiv \frac{v}{U_\infty},\ \phi \equiv \frac{(T - T_\infty)}{(T_o - T_\infty)},\ P \equiv \frac{(p - p_\infty)}{\frac{1}{2}\rho u_\infty^2} \quad (6)$$
$$K_r \equiv K_r^* r_o, K_\theta \equiv K_\theta^* r_o.$$

Using the steam function-vorticity formulation, the non-dimensional form of equations (1-4) is given by:

$$\omega = \nabla^2\psi \quad (7)$$

$$U\frac{\partial\omega}{\partial R} + \frac{V}{R}\frac{\partial\omega}{\partial\theta} = \frac{1}{Re}\nabla^2\omega + \frac{1}{2}\left[-K_\theta\frac{\partial(RV^2)}{\partial R} + K_r\frac{\partial(U^2)}{\partial\theta}\right] \quad (8)$$

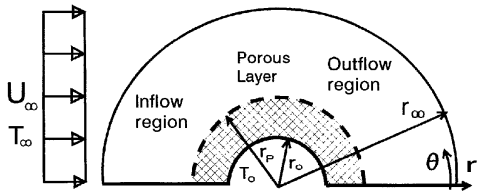


**Figure 1.**
Schematic of the problem

$$U\frac{\partial\phi}{\partial R}+\frac{V}{R}\frac{\partial\phi}{\partial\theta}=\frac{1}{Re\,Pr}\nabla^2\phi \tag{9}$$

where

$$U\equiv\frac{1}{R}\frac{\partial\psi}{\partial\theta},\ V\equiv-\frac{\partial\psi}{\partial R},\ Re\equiv\frac{i_\infty r_o}{\nu},\ Re_D\equiv\frac{u_\infty D}{\nu},\ Pr=\frac{\nu}{\alpha}. \tag{10}$$

In order to resolve accurately the boundary layer around the cylinder, a grid with small radial spacing is required. It is not practical to use this small spacing as we move to the far-stream boundary. Thus, a stretched grid in the radial direction is needed (Anderson, 1994). This will result in unequally spaced nodes and would require the use of more complicated and/or less accurate finite difference formulas. To overcome this problem, the unequally spaced grid in the physical domain (R, $\theta$) is transformed into an equally spaced grid in the computational domain ($\xi, \eta$) (Anderson, 1994), Figure 2. The two domains are related as follows:

$$R=e^{\pi\xi},\theta=\pi\eta. \tag{11}$$

Equations (7-9), along with the corresponding boundary conditions, need to be transformed into the computational domain. In the new computational domain, the current problem will be given by:

$$\omega=\frac{1}{E^2}\left[\frac{\partial^2\psi}{\partial\xi^2}+\frac{\partial^2\psi}{\partial\eta^2}\right] \tag{12}$$

$$\begin{aligned}\frac{\partial^2\omega}{\partial\xi^2}+\frac{\partial^2\omega}{\partial\eta^2}&=\frac{1}{Re}\left[\frac{\partial\psi}{\partial\eta}\frac{\partial\omega}{\partial\xi}-\frac{\partial\psi}{\partial\xi}\frac{\partial\omega}{\partial\eta}\right]\\&-\frac{Re}{2\pi}\left\{-K_\theta\left[\left(\frac{\partial\psi}{\partial\xi}\right)^2+2\frac{\partial\psi}{\partial\xi}\frac{\partial^2\psi}{\partial\xi^2}\right]+2K_r\frac{\partial\psi}{\partial\eta}\frac{\partial^2 so}{\partial\eta^2}\right\}\end{aligned} \tag{13}$$

$$\frac{\partial^2\phi}{\partial\xi^2}+\frac{\partial^2\phi}{\partial\eta^2}=\frac{1}{Re\,Pr}\left[\frac{\partial\psi}{\partial\eta}\frac{\partial\phi}{\partial\xi}-\frac{\partial\psi}{\partial\xi}\frac{\partial\phi}{\partial\eta}\right] \tag{14}$$

$$E=\pi e^{\pi\xi}. \tag{15}$$

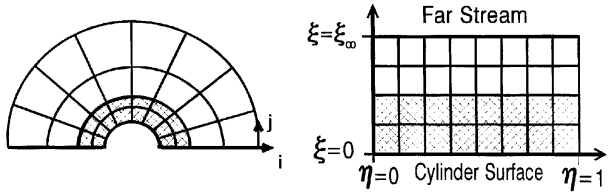


**Figure 2.**
Schematic of the grid in the physical (left) and computational (right) domains

The system of elliptic PDEs given by equations (12)-(14), along with the corresponding boundary conditions, was discretized using the finite difference method. The resulting system of algebraic equations is solved using the hybrid finite differencing scheme (Patankar, 1980). Such a method proved to be numerically stable for convection-diffusion problems. The finite difference form of the equations was checked for consistency with the original PDEs (Patankar, 1980). The iterative solution procedure was carried out until the error in all solution variables ($\psi, \omega, \phi$) became less than a predefined error level ($\in$). Other predefined parameters needed for the solution method included the placement of the far-stream boundary condition ($R_\infty$) and the number of grid points in both radial and tangential directions, N and M, respectively. Extensive testing was carried out in order to determine the effect of each of these parameters on the solution. This was done to insure that the solution obtained was independent of and not tainted by the predefined value of each of these parameters. The testing included varying the value of $\in$ from $10^{-3}$ to $10^{-6}$, $R_\infty$ from 5 to 50, N from 60 to 200, and M from 40 to 120. The results reported herein are based on the following combination: N = 85-100, M = 60, $R_\infty$ = 20, and $\in = 10^{-5}$. The variation in the number of grid points used in the radial direction was a function of the thickness of the porous layer. The variation was to insure that the edge of the porous layer coincided with one of the grid's radial lines, see Figure 2. The current gird resolution used is similar or better than most grids used in published studies of natural convection (Saitoh *et al.*, 1993), forced convection (Ahmad, 1996), and mixed convection heat transfer (Badr, 1983; Abu-Hijleh, 1999). Figure 3 shows very good agreement between the average Nusselt number calculated by the current code and different results reported in the literature (Ahmad, 1996; Badr, 1983; Abu-Hijleh, 1999; Incropera, 1996), for the case of a smooth cylinder without a porous layer.

## Results

The changes in the forced convection heat transfer from an isothermal cylinder covered with a porous layer in cross-flow was studied for several combinations

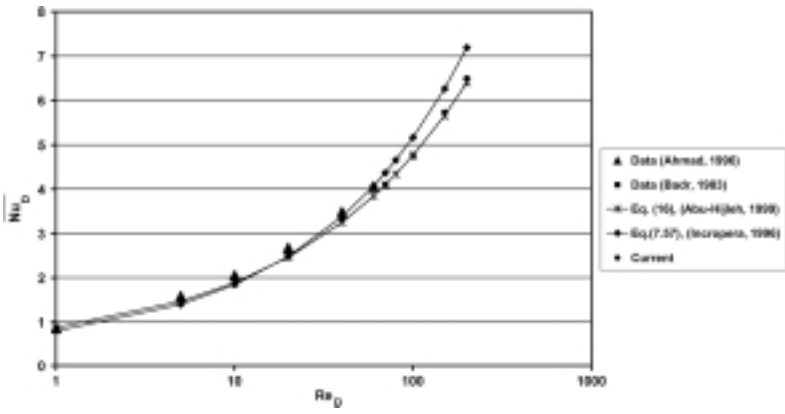


**Figure 3.**
Comparison of the average Nusselt number for the case of a smooth cylinder

of non-dimensional porous layer radius (Rp = 1.1, 1.2, 1.35, 1.5, 1.75, 2.0), non-dimensional porous resistances ($K_r$ and $K_\theta$ = 0.25, 0.5, 1.0, 1.5, 2.0), and Reynolds number ($Re_D$ = 1, 5, 10, 20, 40, 70, 100, 150, 200). This resulted in more than 1,350 distinct runs excluding the several verification runs reported in the previous section. The change in the average Nusselt number, at a given value of Reynolds number, due to the addition of the porous layer ($\overline{Nu}_{D,P}$) was normalized by the average Nusselt number of a smooth cylinder, no porous layer ($R_P$ = 1.0 and $K_r = K_\theta$ = 0.0), at the same Reynolds number ($\overline{Nu}_D$).

Figure 4 shows the change in the normalized average Nusselt number as a function of the radial non-dimensional resistance ($K_r$) at selected values of $K_\theta$, $Re_D$, and $R_p$. It can be seen that $K_r$ has a minimal effect on the changes in the normalized average Nusselt number. It is only at high values of $Re_D$ and $R_P$ and low values of $K_\theta$ that changing $K_r$ results in a noticeable change in the Nusselt number. As expected, increasing $K_r$ reduces Nusselt. The increased porous layer resistance reduces the air speed near the hot cylinder surface which in turn reduces the convection heat transfer from the cylinder, thus the lower Nusselt number. This is expected as the porous layer will reduce the air velocity over the cylinder surface which in turn will reduce the forced convection heat transfer from the cylinder. Near the cylinder surface, the air velocity is predominantly in the tangential component. The magnitude of the extra pressure loss due to the porous layer radial resistance is dependent on the radial velocity component only, equation (2). This explains the ineffectiveness of the porous layer radial resistance in terms of changing the Nusselt number.

Figure 5 show the change in the normalized average Nusselt number as a function of the tangential non-dimensional resistance ($K_\theta$) at selected values of $K_r$, $Re_D$, and $R_p$. The reduction in the Nusselt number as a function of the tangential porous layer resistance is greater than that caused by the radial resistance. This is due to the dominance of the tangential velocity component near the cylinder surface and the dependence between the pressure loss due to the porous layer's tangential resistance and the tangential velocity, equation (3). The reduction in Nusselt number increases as $Re_D$ and $R_P$ increase. The increase in $Re_D$ indicates that the incoming flow has a high speed. Recalling equations (2) and (3), the porous layer resistance is proportional to the square of the air speed. Thus the effectiveness of the porous layer will be higher as $Re_D$ increases. Increasing the porous layer thickness increases the contact area between the incoming flow and the porous layer. This in turn increases the pressure loss due to the presence of the porous layer. The increase in the pressure loss also causes the flow to separate from the cylinder surface at an earlier tangential location. This increases the low speed recirculation zone behind the cylinder in which the local Nusselt number will be low. Figure 6 shows the streamline and isothermal contours at different values of $K_\theta$. The minimal effect of $K_r$, reported in Figure 4, can also be seen in Figure 5.

Figure 7 shows the change in the normalized average Nusselt number as a function of the porous layer thickness ($R_P$) at selected values of $K_r$, $K_\theta$, and $Re_D$. As the porous layer thickness increases the Nusselt number decreases. The

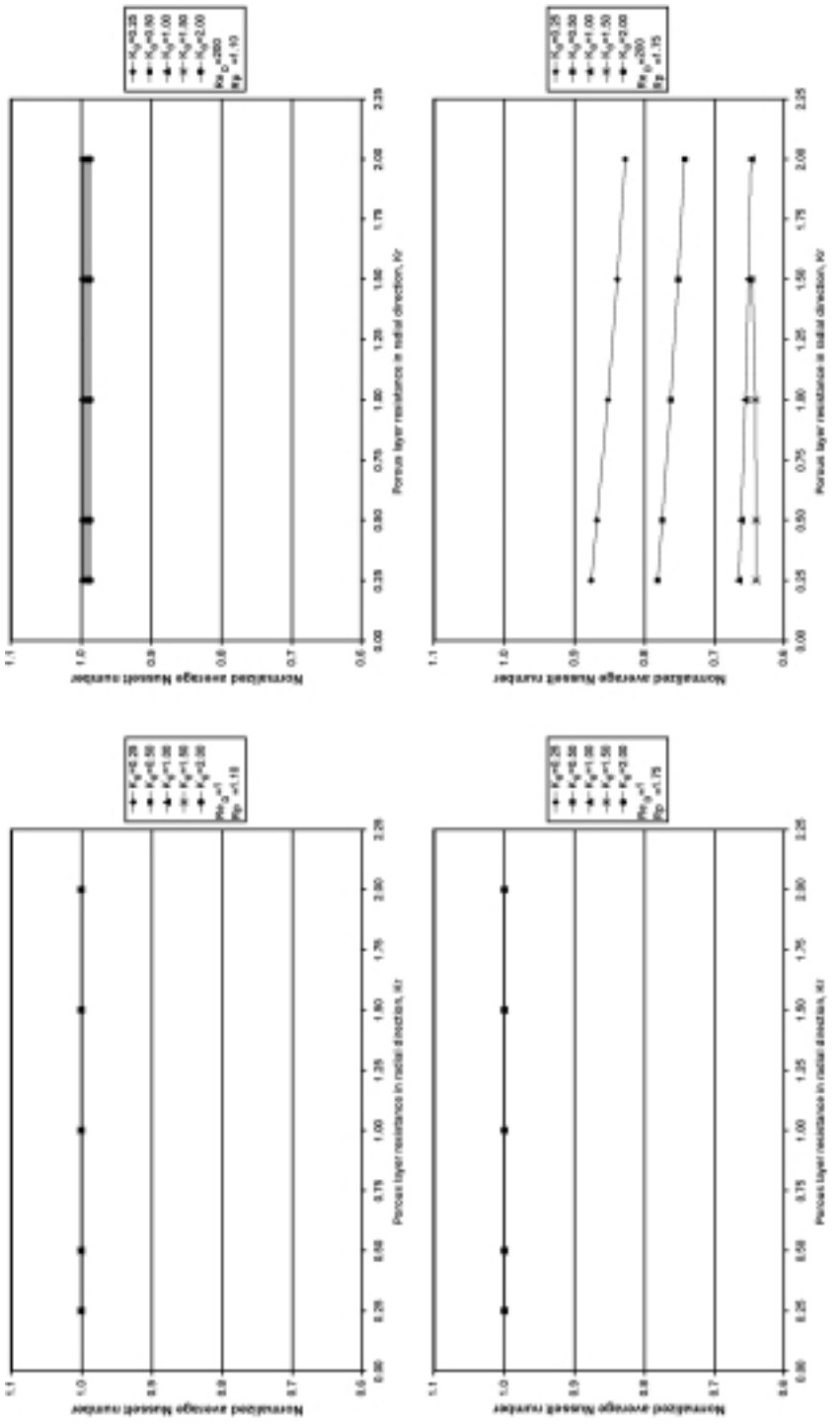

**Figure 4.**
Change in the normalized average Nusselt number as a function of porous layer radial resistance

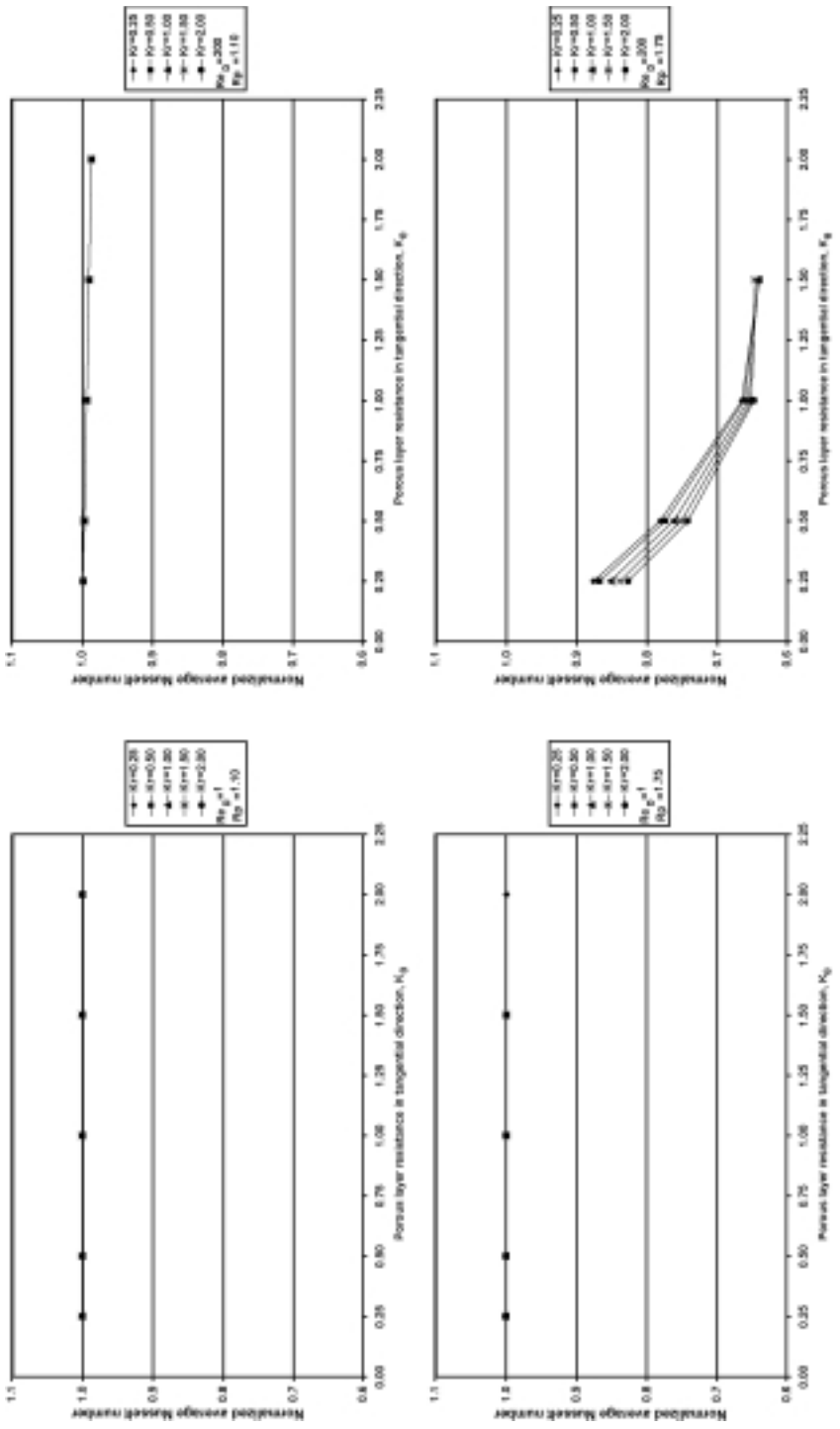

**Figure 5.**
Change in the normalized average Nusselt number as a function of porous layer tangential resistance

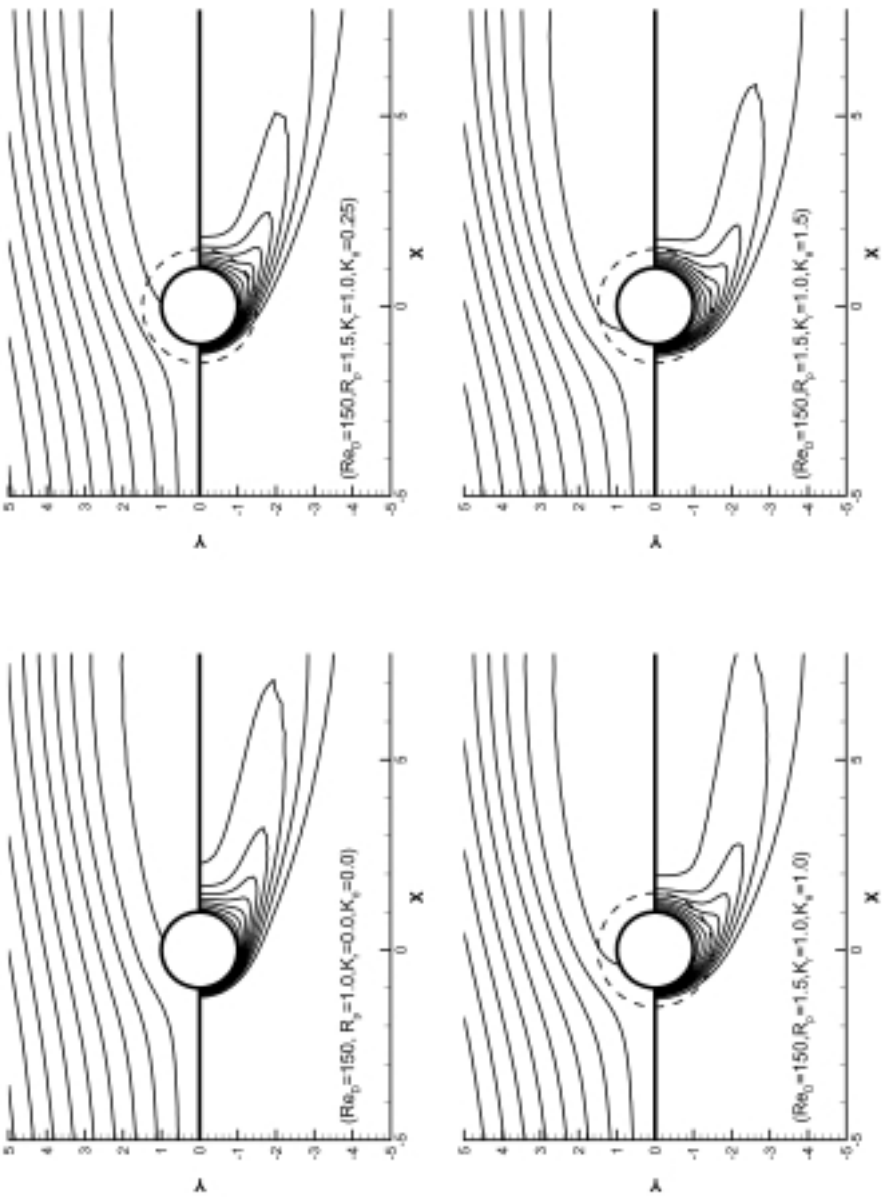


**Figure 6.**
Streamline (top) and isothermal (bottom) contours for the cases ($Re_D$, $R_p$, $K_r$, $K_\theta$: (150,-,-,-), (150, 1.5, 1.0, 0.25), (150, 1.5, 1.0, 1.0), and (150, 1.5, 1.0, 1.5)

reduction in the normalized average Nusselt number was as much as 40 per cent depending on the combination of $Re_D$ and porous layer thickness and resistance. This is due to the increased area of contact between the porous layer and incoming flow which in turn reduced the speed of air in the vicinity of the cylinder and the resulting heat transfer from the cylinder surface. Note that not all curves are complete. The code did not converge for combinations of large

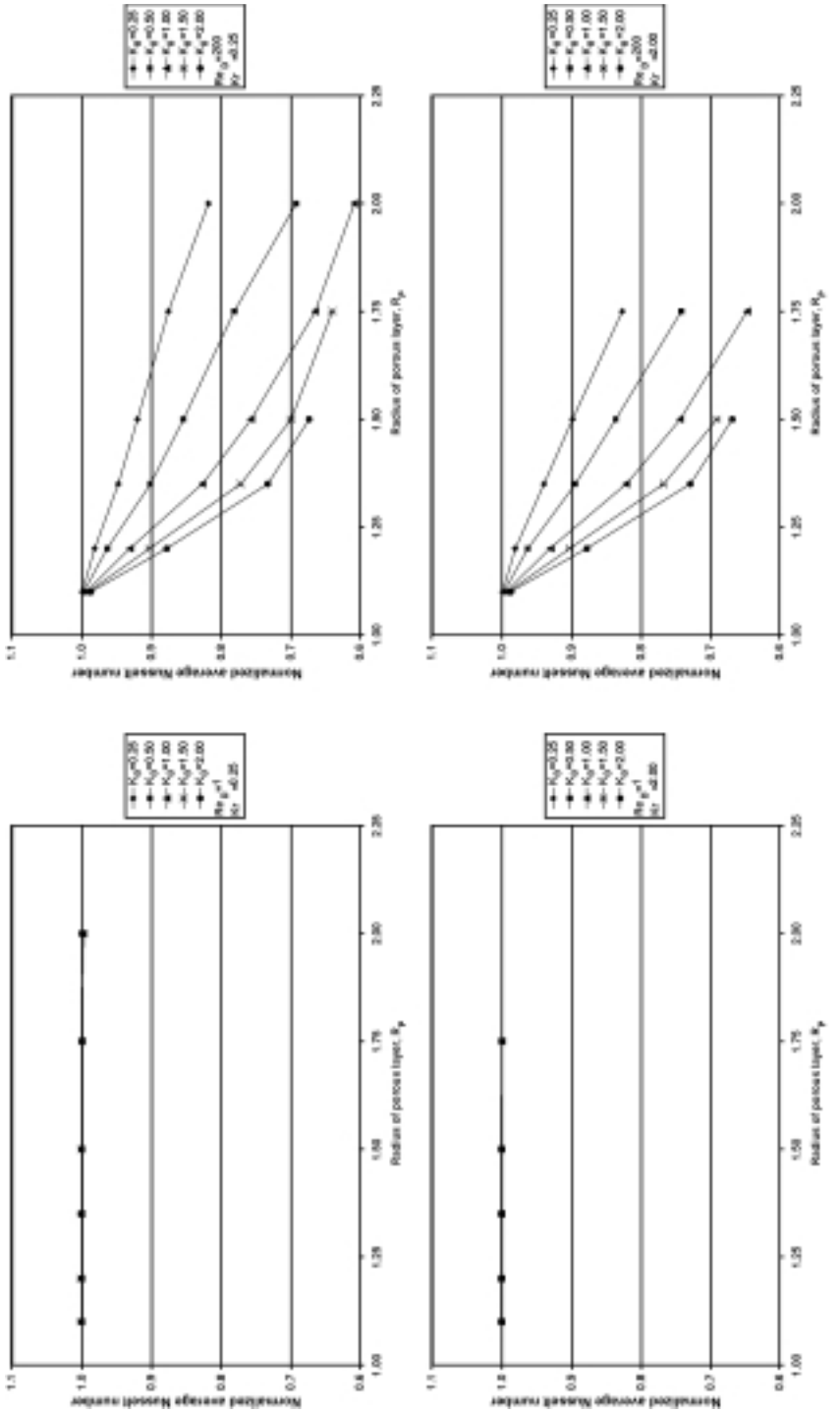

**Figure 7.**
Change in the normalized average Nusselt number as a function of porous layer thickness

porous layer thickness and resistance. Figure 8 shows the streamline and isothermal contours at different values of $R_p$. The changes in the separation location and the increase in the recirculation zone behind the cylinder as a function of porous layer thickness are clear in this figure.

Figure 9 shows the change in the normalized average Nusselt number as a function of Reynolds number ($Re_D$) at selected values of $R_P$, $K_r$, and $K_\theta$. The Nusselt number decreases with increasing Reynolds number. From equations (2)

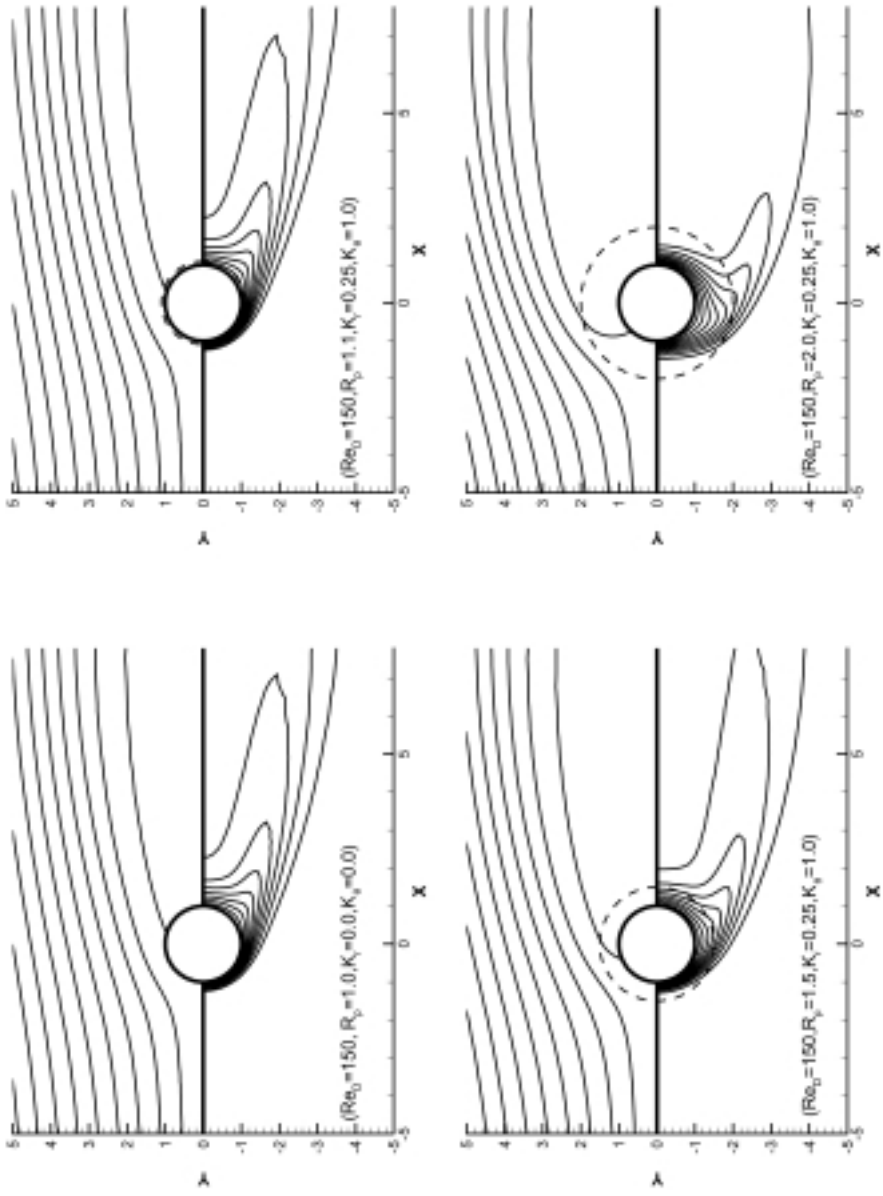


**Figure 8.**
Streamline (top) and isothermal (bottom) contours for the cases ($Re_D$, $R_p$, $K_r$, $K_\theta$: (150,-,-,-), (150, 1.1, 0.25, 1.0), (150, 1.5, 0.25, 1.0), and (150, 2.0, 0.25, 1.0)

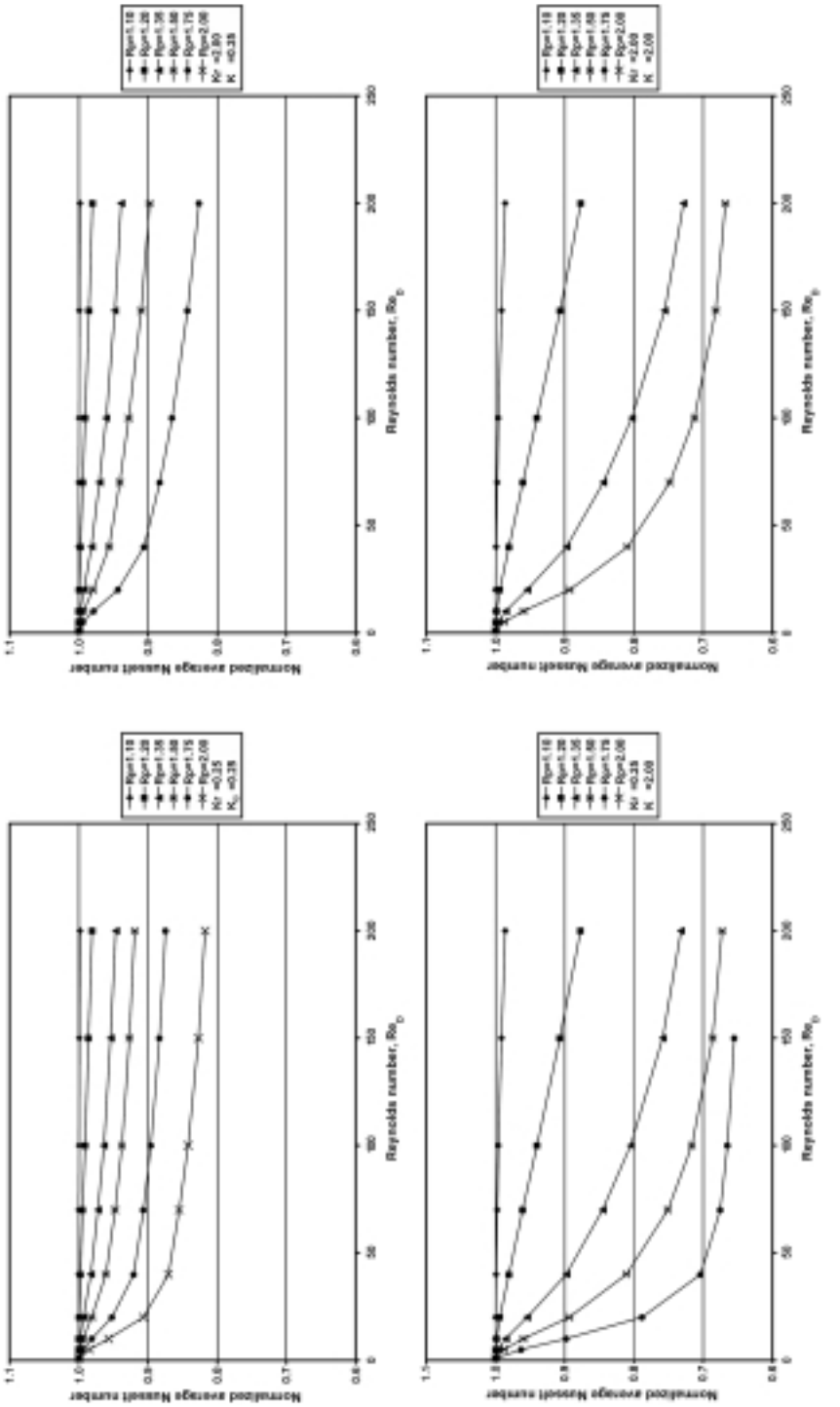


**Figure 9.**
Change in the normalized average Nusselt number as a function of Reynolds number

and (3), an increase in the air speed results in higher pressure losses in the momentum equations. This in turn reduces the heat transfer from the cylinder. The relative effectiveness of the tangential resistance compared to that of the radial resistance is clearly visible.

## Conclusions

The problem of laminar cross-flow forced convection heat transfer from an isothermal horizontal cylinder covered with an orthotropic porous layer was studied numerically. Changes in the normalized average Nusselt number at different combinations of non-dimensional porous layer thickness ($R_p$), radial and tangential resistances ($K_r$ and $K_\theta$), and Reynolds number ($Re_D$) were reported. The Nusselt number decreased, as much as 40 per cent, with increasing porous layer thickness and/or resistance. The reduction in the normalized average Nusselt number was predominately a function of the changes in the tangential resistance ($K_\theta$). The radial resistance ($K_r$) had little effect of the Nusselt number. The porous layer was most effective in reducing the Nusselt number at high values of Reynolds number.

### References

Abu-Hijleh, B.A/K. (1999), "Laminar mixed convection correlations for an isothermal cylinder in cross flow at different angles of attack", *International Journal of Heat Mass Transfer*, Vol. 42, pp. 1383-8.

Abu-Hijleh, B.A/K. (n.d.), "Natural convection heat transfer from a cylinder with an orthotropic porous layer", Submitted to the *International Journal of Heat and Fluid Flow*.

Ahmad, R.A. (1996), "Steady-state numerical solution of the Navier-Stokes and energy equations around a horizontal cylinder at moderate Reynolds numbers from 100 to 500", *Heat Transfer Engineering*, Vol. 17, pp. 31-81.

Alazmi and Vafai (2000), "Analysis variants within the porous media transport models", *Journal of Heat Transfer*, Vol. 122, pp. 303-26.

Al-Nimr, M.A. and Alkam, A.K. (1998), "A modified tubeless solar collector partially filled with porous substrate", *Renewable Energy*, Vol. 13, pp. 165-73.

Anderson, J.D. (1994), *Computational Fluid Dynamics: The Basics with Applications*, McGraw-Hill, New York, NY.

Badr, H.M. (1983), "A theoretical study of laminar mixed convection from a horizontal cylinder in a cross stream", *International Journal of Heat Mass Transfer*, Vol. 26, pp. 639-53.

Kuznetsov, A.V. (2000), "Analytical studies of forced convection in partly porous configurations", in Vafai, K. (Ed.), *Handbook of Porous Media*, Marcel Dekker, New York, NY, pp. 269-312.

Huang, P.C. and Vafai, K. (1994), "Flow and heat transfer control over an external surface using a porous block array arrangement", *International Journal of Heat Mass Transfer*, Vol. 36, pp. 604-13.

Idelcik, I.E. (1994), *Handbook of Hydraulic Resistance*, 3rd ed., CRC Press, Boca Raton, FL.

Incropera, F.P. and DeWitt, D.P. (1996), *Fundamentals of Heat and Mass Transfer*, John Wiley & Sons, New York, NY.

Martin, A.R., Satiel, C. and Shyy, W. (1998), "Heat transfer enhancement with porous inserts in recirculating flow", *Journal of Heat Transfer*, Vol. 120, pp. 458-67.

Morgan V.T. (1975), "The overall convective heat transfer from smooth circular cylinders", *Advanced Heat Transfer*, Vol. 11, pp. 199-264.

Ochoa-Tapia, J.A. and Whitaker, S. (1995a), "Momentum transfer at the boundary between a porous medium and a homogenous fluid – I. Theoretical development", *International Journal of Heat Mass Transfer*, Vol. 38, pp. 2635-46.

Ochoa-Tapia, J.A. and Whitaker, S. (1995b), "Momentum transfer at the boundary between a porous medium and a homogenous fluid – II. Comparison with experiment", *International Journal of Heat Mass Transfer*, Vol. 38, pp. 2647-55.

Patankar, S.V. (1980), *Numerical Heat Transfer of Fluid Flow*, McGraw-Hill, New York, NY.

Saitoh, T., Sajik, T. and Maruhara, K. (1993), "Benchmark solutions to natural convection heat transfer problem around a horizontal circular cylinder", *International Journal of Heat Transfer*, Vol. 36, pp. 1251-9.

Zhang, B. and Zhao, Y. (2000), "A numerical method for simulation of forced convection in a composite porous/fluid system", *International Journal of Heat Fluid Flow*, Vol. 21, pp. 432-41.